Applied Radiation and Isotopes 225 (2025) 112090

Contents lists available at ScienceDirect

Applied Radiation and Isotopes

journal homepage: www.elsevier.com/locate/apradiso

X-ray tube design optimization methods based on CST particle studio

Hao Yu [a], Yunpeng Liu [a,b,*], Junxu Mu [a], Jiaxin Bai [a], Ao Xia [a], Xiushan Wang [a], Xiaobin Tang [a,b]

[a] Department of Nuclear Science and Technology, Nanjing University of Aeronautics and Astronautics, Nanjing, 210016, China
[b] Key Laboratory of Advanced Nuclear Technology and Radiation Protection, Ministry of Industry and Information Technology, Nanjing, 210016, China

ARTICLE INFO

Keywords:
Optimization technique
NSGA-II
X-ray tube
Focal spot

ABSTRACT

This work aims to enhance the optimization of X-ray tubes, focusing on improving the accuracy of the focal spot and optimizing time characteristics. Three optimization techniques are compared: Parameter Sweep (Par. Sweep), Automatic Optimization (Optimizer), and Non-Dominated Sorting Genetic Algorithm II (NSGA-II), applied to X-ray tube designs using CST Particle Studio. The results show that while Par. Sweep achieves a focal spot radius of 0.82 mm and Optimizer achieves 0.31 mm, NSGA-II demonstrates the most significant improvement, with a focal spot radius of 0.17 mm—resulting in a 79.3 % and 45.2 % improvement in spatial resolution compared to Par. Sweep and Optimizer, respectively. Although NSGA-II consumes ten times more computational resources than Optimizer, it offers a range of structural design solutions to accommodate the diverse performance requirements of users. For instance, one NSGA-II design option reduces the X-ray tube transit time to 0.71 ns. These findings underscore the potential of NSGA-II in achieving more precise X-ray tube optimization and its applicability to the development of other vacuum electronic devices.

1. Introduction

X-ray tube is a vacuum electronic device that converts electrons into X-rays and is widely used in material characterization, non-destructive testing, and medical imaging (Figueroa et al., 2021; Parmee et al., 2015). Among these applications, high-speed X-ray imaging, which demands fast temporal resolution and high imaging clarity, places stringent requirements on the tube current, focal spot, and temporal characteristics of X-ray tubes. However, owing to the complexity of the manufacturing process and high precision requirements of the X-ray tube, the research and development cycle and costs are significant. Thus, the rapid development of such devices is challenging. Numerical simulation technology can fully simulate the physical processes of X-ray tubes, thereby improving device structure design and saving time and cost (Antonsen et al., 1999).

CST Particle Studio (CST PS) can accurately simulate the motion trajectories of particles in complex electromagnetic fields and is widely used in the design of vacuum electronic devices. The three-dimensional trajectories of electrons in CST PS are computed by numerically integrating the relativistic equations of motion under the Lorentz force, using electromagnetic fields obtained from full-wave solvers or external sources. Currently, the main optimization design methods for X-ray tubes based on CST PS include parameter scanning (Par. Sweep) and automatic optimization routines. Par. Sweep involves calculating and analyzing the effects of various parameters on device performance, summarizing patterns, and selecting the best structural parameters to achieve optimization. Tan et al. (2019) used CST PS for the parameter optimization design of a distributed X-ray source. They employed Par. Sweep to investigate the influence of parameters, such as the electrode voltage of two electrostatic lenses, on electron emission and deflection. They found that when the electrode voltages were 8 and 11 kV, the electron beam had a minimum focal spot of 0.85 mm. Gui et al. (2015) optimized the electrostatic focusing lens of a carbon nanotube cathode X-ray source by studying the electron beam size under different focusing voltages and different lengths of the long and short axes of the focusing aperture. They reported that the optimal focusing voltage was 1000 V, and the best aperture size was 20 mm × 24 mm for the optimal focusing structure. However, attaining globally optimal parameters is hindered by the local optima caused by Par. Sweep. Additionally, CST PS provides an automatic optimization routine (Optimizer). Optimizer can automatically optimize the vacuum electronics design within a given parameter range by setting target performance and can determine the best structural parameters to achieve the desired performance. Gao et al. (2024) minimized the electron focal spot size of an X-ray source using

* Corresponding author. Department of Nuclear Science and Technology, Nanjing University of Aeronautics and Astronautics, Nanjing, 210016, China.
E-mail address: liuyp@nuaa.edu.cn (Y. Liu).

https://doi.org/10.1016/j.apradiso.2025.112090
Received 27 August 2024; Received in revised form 30 April 2025; Accepted 7 August 2025
Available online 8 August 2025

Optimizer by adjusting the positional parameters and magnetic field gradients of the focusing magnet. As a result, an electron focal spot size of approximately 1.2 mm × 1.2 mm was achieved at a tube voltage of 20 kV. Although Optimizer can rapidly achieve a certain degree of automatic optimization, it targets achieving a predetermined effect or a preset goal. However, in a real-world scenario, the optimal performance of a device is unknown; thus, the predetermined goal may not be achieved, or the structural parameters to achieve the goal may not be optimal.

Owing to their suitability for optimizing the design of vacuum electronics, non-dominated sorting genetic algorithm-II (NSGA-II) is widely used to solve multi-objective optimization problems. Srinivas and Deb (1994) proposed the non-dominated sorting genetic algorithm (NSGA) in 1994. NSGA-II is a fast non-dominated sorting algorithm based on NSGA, and it adopts an elite strategy. It introduces the concept of congestion, which helps increase the operating speed and robustness of the algorithm (Deb et al., 2002). NSGA-II and CST PS can jointly perform simulation and optimization of vacuum electronic apparatuses (Li et al., 2023; Feng et al., 2022) and effectively achieve the structural parameter design corresponding to the optimal performance of the apparatus. In this study, an X-ray tube model was built based on the CST PS. The performances of three different optimization algorithms—parametric scanning, Optimizer, and NSGA-II—were compared and analyzed by studying the variation in the focal spot and time characteristics of the optimized X-ray tube. Among them, the optimization method based on NSGA-II combined with CST PS requires only a few manual steps to obtain a more flexible and superior design solution for device optimization with high accuracy. The method can be extended to other types of vacuum electronic devices, such as magnetrons, accelerating tubes, thereby accelerating the design process and promoting the rapid development of new devices.

2. Modeling optimal objects

2.1. X-ray tube structure

An X-ray tube, as a typical vacuum electronics device, consists of an electron-emitting cathode and an electron-collecting anode. It may additionally constitute a focusing structure between the cathode and anode to restrict the electron trajectory. Unlike in other vacuum electronic devices, the anode of the X-ray tube converts electron energy into X-rays. As shown in Fig. 1, the anode has an inclined surface. The electrons entering from the left collide against the anode, are converted into X-rays, and are emitted from the lower exit (Fox and Hyoung, 2024).

2.2. Electron focusing

In most vacuum electronic equipment, electron focusing is considered to change the trajectory of electrons or collect the maximum possible electrons at the anode end. The circular focusing ring is a typical focusing structure. In an axisymmetric electrostatic field, the law of electron motion follows the Laplace equation

$$\frac{\partial^2 V}{\partial Z^2}+\frac{1}{\mathrm{r}}\frac{\partial}{\partial r}\left(r\frac{\partial V}{\partial r}\right)=0, \tag{1}$$

where $V=V(z,r,\theta)$ is the potential function in the electrostatic field. Equation (1), when solved based on the boundary conditions, produces the Scherch series (Jiye, 1987) under the paraxial condition as

$$V(z,r)=\phi(z)-\frac{1}{4}\phi''(z)r^2+\frac{1}{64}\phi^{(4)}(z)r^4, \tag{2}$$

where $\phi(z)$ is the potential distribution on the axis. According to this equation, the potential function of any point in the axisymmetric electrostatic field $V(z,r)$ can be obtained through the coordinates, $\phi(z)$ and its derivatives, following which the spatial potential distribution in the vacuum electronic device can be obtained. The component Er of the electric field intensity in the radial direction can be obtained by differentiating Equation (2) as follows:

$$Er=-\frac{\partial V}{\partial r}=\frac{1}{2}\phi''(z)r. \tag{3}$$

Therefore, the radial force on the electrons can be given by

$$Fr=-\frac{e}{2}\phi''(z)r. \tag{4}$$

The distribution of the axial electric field in the X-ray tube without and with a focusing system is shown in Fig. 2(a) and (b), respectively. As shown in Fig. 2(b), the addition of a focusing system between the cathode and anode results in the bending of the electric field lines in this area, and $\phi''(z)>0$ can be deduced. Therefore, $Fr<0$ from Equation (4). That is, the radial force on the electron moves inward along the radial direction. Fig. 2(c) and (d) respectively show the electron motion trajectory without and with the focusing ring. Evidently, the addition of a focusing ring is conducive to obtaining a concentrated electron beam.

Changes in the focusing structure alter the potential distribution in the space, which affects the electron trajectory. Therefore, the optimal design of the focusing structure is of great significance for the overall optimal design of the vacuum electronic equipment.

2.3. Optimal parameters

In an X-ray tube, the focusing and anode structure design directly affect the electron trajectory, thereby impacting the X-ray output performance.

As shown in Fig. 3, the $z=0$ plane is used as the cathode electron emission surface. In this study, we focused on optimizing the focus ring and anode structure and position parameters: z_b is the starting position of the focus ring, z_e is the ending position of the focus ring, r_{in} is the inner radius of the focus ring, d_{fs} is the distance between the focus ring and

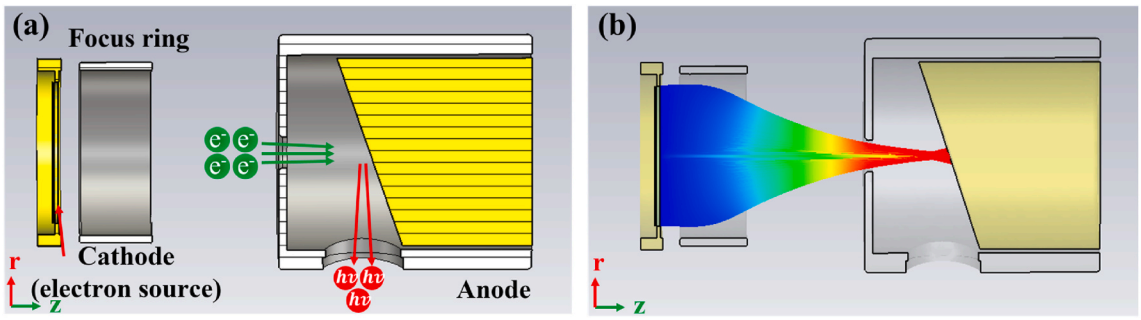

Fig. 1. Electron flight inside an X-ray tube. (a) Basic structure of an X-ray tube. (b) Simulated electron trajectories inside the tube, obtained using the particle tracking solver integrated in CST PS.

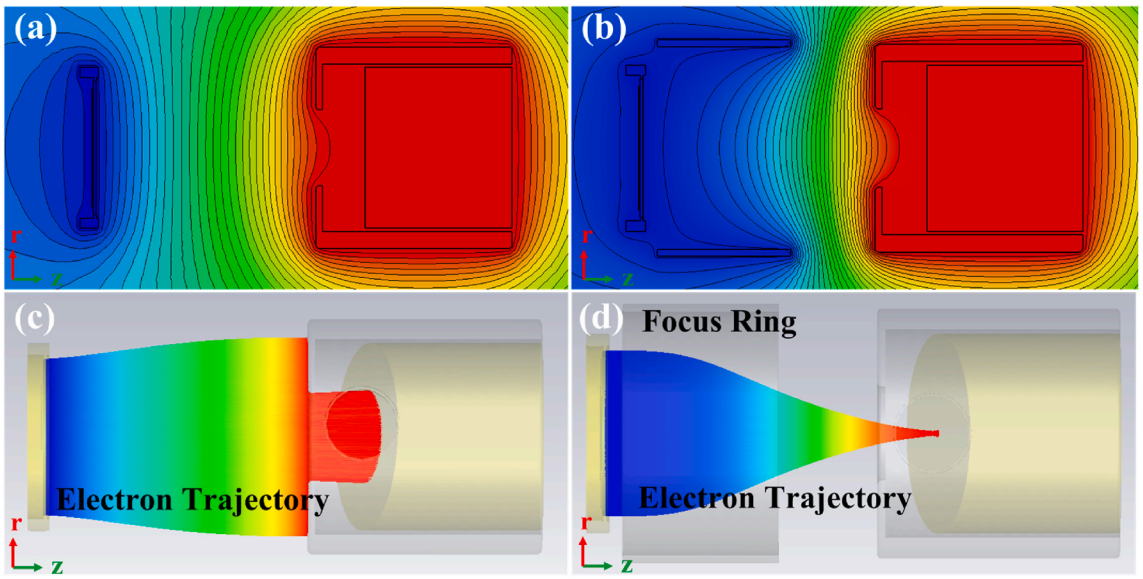

Fig. 2. Potential and electron trajectory inside the X-ray tube with and without a focusing system. (a) Potential distribution without focusing. (b) Potential distribution with focusing. (c) Electron trajectory without focusing. (d) Electron trajectory with focusing. (Trajectories are obtained through the particle tracking solver integrated within CST PS).

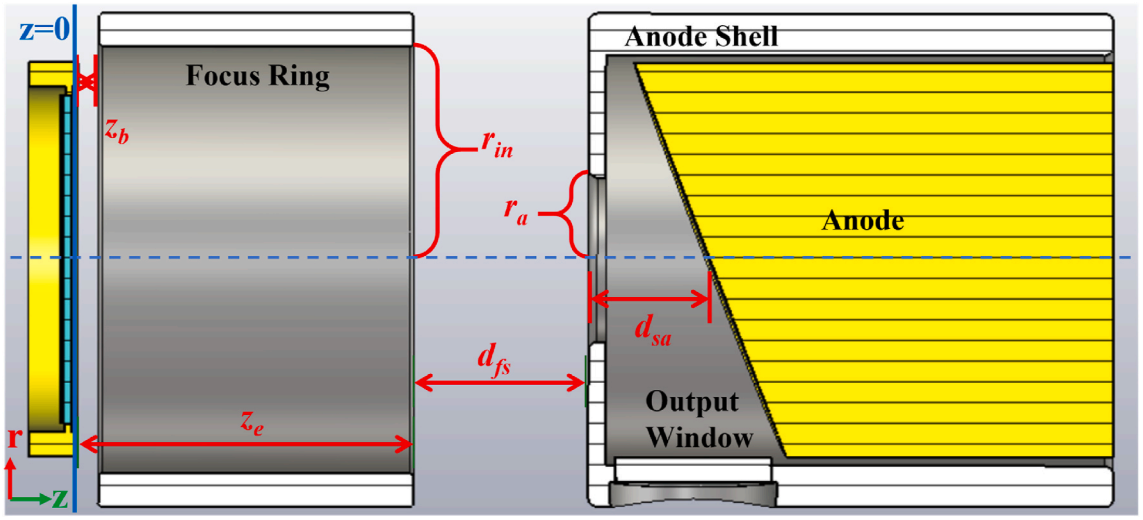

Fig. 3. Structural parameters that need to be optimized in the X-ray tube.

anode cover, r_a is the opening radius of the anode cover, and d_{sa} is the distance between the top of the anode cover and anode center. These parameters were coupled to each other and jointly affected the electron motion trajectory. Here, the initial structural parameters were $z_b = 2$ mm, $z_e = 20$ mm, $r_{in} = 10$ mm, $d_{fs} = 15$ mm, $r_a = 5$ mm, and $d_{sa} = 10$ mm.

2.4. Optimal targets

2.4.1. Electron collection rate

The ratio (R_e) of the number of electrons collected by the anode to the initial number of electrons emitted by the cathode electron source indicates the probability of electrons reaching the anode from the cathode. For most vacuum devices, such as electron guns and X-ray tubes, R_e should be as large as possible to ensure the maximum number of electrons reach the anode. In subsequent comparisons and calculations, the initial number of electrons was set to 16358.

2.4.2. Focus spot size

The electron focus size (R_{fs}) is an evaluation indicator of the performance of vacuum electronic devices. In CST PS, a particle monitoring surface can be set up near the anode to intercept the shape of the electron trajectory in space on this surface to obtain the electron focus. Fig. 4 shows the definitions of electron focus, actual focus, and effective focus in the X-ray tube. The electron focus indicates the projection of the actual focus on the inclined surface of the anode target in the electron flight direction. The electron focus can be converted into an effective focus by the target angle. The effective focus characterizes the spatial resolution of the X-ray tube and directly affects the resolution of the X-ray imaging (Ihsan et al., 2007).

2.4.3. Time characteristics

The time characteristics of vacuum electronics mainly include transit time (*TT*) and transit time spread (*TTS*) (Hang et al., 2018). *TT* is the time interval between the peaks of the input and output signals; it represents the degree of delay of the output signal relative to the input

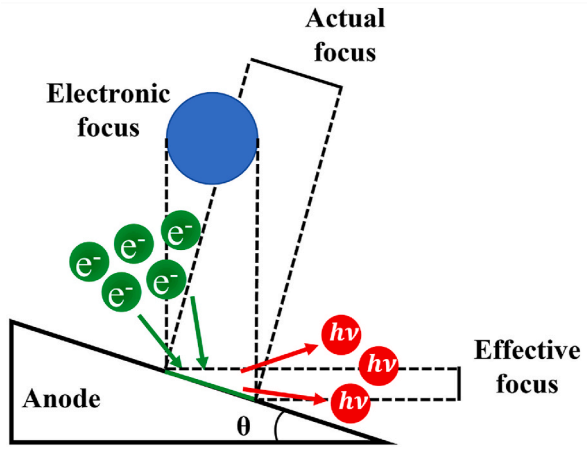

Fig. 4. Representation of electron, actual, and effective focal spots in an X-ray tube.

signal. *TTS* is the degree of widening of the half-width of the output signal compared with the half-width of the input signal. In vacuum electronic devices, *TTS* is mainly caused by the difference in the trajectory and speed of electron motion. As shown in Fig. 5, when the input signal is a $\delta(t)$ pulse (the unit electron pulse amplitude function generated by the electron source), the half-width of the output signal ($t_2 - t_1$) can directly represent *TTS*, and *TT* can be represented by $t_o - t_i$. Here, t_i denotes the time of signal generation, t_o is the time at which the output signal reaches its peak intensity, and t_1 and t_2 correspond to the times when the output signal intensity decreases to half of its peak value.

The time characteristic is of great significance for vacuum electronic assemblies, such as photomultiplier tubes, which require ultrafast response. In X-ray tubes, the time characteristic mainly affects the outgoing X-ray pulse modulation rate. In terms of optimization, an X-ray tube design with the smallest possible *TT* and *TTS* is desirable.

3. Simulation results and discussion

3.1. Parameter sweeping

Par. Sweep module is a powerful way to quickly analyze the effect of changes in structural parameters on the simulation results. The optimal parameter values can be determined by comparing the simulation results using different parameters. First, we attempted to optimize z_b, the starting position of the focus ring. The influence of the change in z_b on the electron focus was explored by setting the initial value $z_b = 2$ mm, sweep interval = 1–10 mm, and step size = 1 mm.

Fig. 6(a)–(d) show the shapes of the electron focuses corresponding to $z_b = 2$, 3, 4, and 5 mm, respectively. Since the electron source on the cathode is circular and the internal electric field of the X-ray tube is symmetric about the z-axis, the electron focus is approximately circular. As the starting position of the focus ring increases its distance from the cathode, the electron beam transitions from an overfocused state to an underfocused state, resulting in the electron focus initially decreasing and then increasing in size. For $z_b \approx 4$ mm, the X-ray tube obtained the best $R_{fs} = 2.20$ mm.

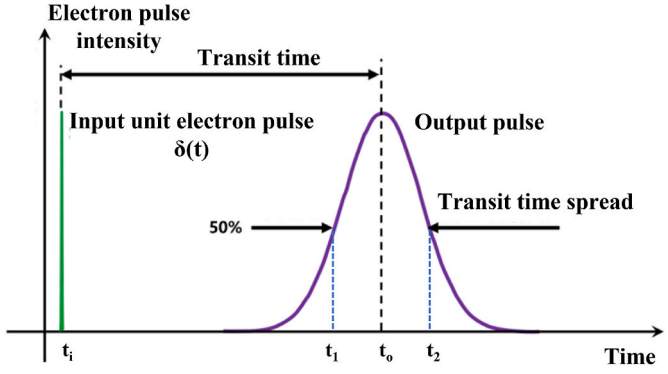

Fig. 5. Definition of transit time and transit time spread.

To explore the effect of the focusing-ring length on the focal spot, the end position z_e of the focusing ring was scanned and analyzed with an optimized parameter $z_b = 4$ mm, with a scanning interval = 6–20 mm and step size = 1 mm. The significance of the optimal length is that if the length deviates from its suitable value, the focusing ring may overfocus or defocus the electron beam.

As can be inferred from Table 1, an optimum focal spot of 0.82 mm was obtained for the X-ray tube at $z_e = 9$ mm. After two parameter scans, the focal spot radius was reduced from the initial 4.00 mm–2.20 mm and then to 0.82 mm. Thus, $z_b = 4$ mm and $z_e = 9$ mm were identified as the appropriate set of structural parameters. In this process, parameter scanning played a certain optimization role, but the obtained structural parameters were not optimal. This is because the coupling relationship between z_b and z_e was ignored. When the parameter scan of z_e value was performed with optimized parameter $z_b = 4$ mm as the initial value, the entire optimization target fell into the local optimum (Cai et al., 2020). Moreover, only the focal spot size was targeted here. With the increase in the number of optimization targets, it became challenging to perform parameter scanning and obtain convincing results.

3.2. Optimizer

Optimizer is an automatic optimization program provided by CST PS. It allows for the parameterization of models, enabling users to find the optimal design parameters to achieve a desired effect or specific objective.

Optimizer comprises both local and global optimization algorithms. Local optimizers provide fast but local minimum optimization, rather than the overall best solution (Mistry et al., 2019). Conversely, global optimizers can search the entire problem space but generally require more computations.

z_b, z_e, and r_{in} were used as the optimization parameters, with R_e and R_{fs} as the optimization targets (Optimizer 1). Optimizer has a built-in genetic algorithm. The population (*pop*), number of generations (*gen*), and mutation rate were set to 50, 50, and 0.6, respectively, and the optimization intervals for the parameters z_b, z_e, and r_{in} were in the range of 1–10, 6–20, and 8–15 mm, respectively. Before the commencement of optimization, the specific values of the optimization targets must be set under the "goals" column of Optimizer. The preset value of R_{fs} was less than 0.5 mm and that of the number of electrons collected by the anode was 16358 ($R_e = 100$ %).

The calculation took 33039 s, and the results are shown in Fig. 7(a). At $R_e = 100$ %, the minimum R_{fs} was 0.60 mm. At this time, z_b, z_e, and r_{in} were 1.2893, 11.5570, and 10.5312 mm, respectively. The results did not meet the preset goal of $R_{fs} < 0.5$ mm, which may be due to the insufficient population and generation or considerably few optimization parameters. However, these results were still better than those obtained by direct parameter scanning.

Using the six structural parameters (Section 2.3) as optimization parameters and the three performance indicators (Section 2.4) as optimization targets (Optimizer 2), additional optimization targets for time performance were set in the goals, and *TT* was required to be < 1 ns. Other conditions remained the same as in the previous step.

The computation was completed in 1697 s after reaching the preset goals in round 54. The corresponding results are shown in Fig. 7(b) and (c). Under the premise that R_e reaches 100 %, both R_{fs} and *TT* results met the preset targets with specific values of 0.31 mm and 0.98 ns, respectively. At this time, the structural parameters were $z_b = 2.48242$, $z_e = 21.76175$, $r_{in} = 14.59871$, $d_{fs} = 12.19335$, $r_a = 5.64331$, $d_{sa} = 6.75818$. Here, the obtained $R_{fs} = 0.31$ mm was 62.2 % and 48.3 % less than the

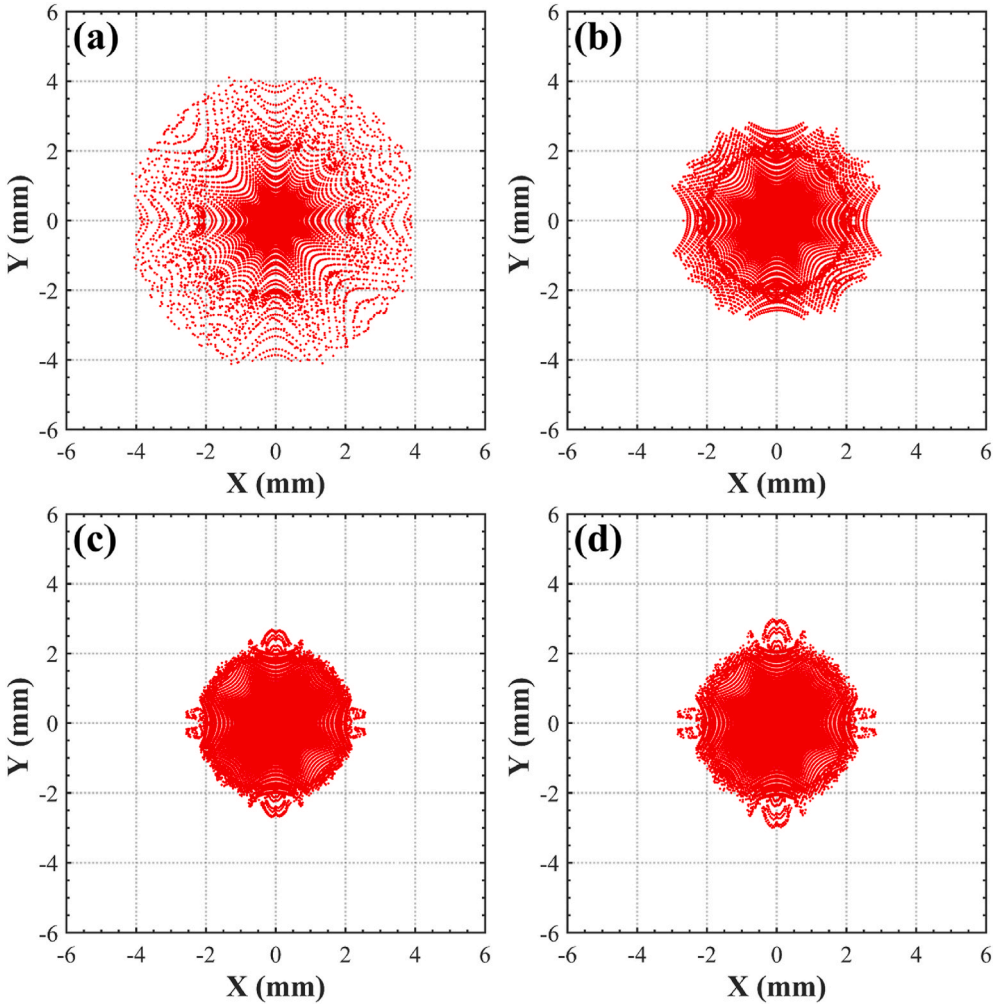

Fig. 6. Focus spot shapes at different starting positions of focus rings. z_b = (a) 2 mm, (b) 3 mm, (c) 4 mm, and (d) 5 mm.

Table 1
R_{fs} corresponding to z_e values (partial results).

z_e (mm)	R_{fs} (mm)
6	2.43
7	1.74
8	1.22
9	0.82
10	0.90
11	1.04
12	1.14

results obtained by parameter scanning and three-parameter two-optimization target optimization, respectively. However, this value was possibly not the optimal value of the device performance. It only achieved the established effect in Optimizer and realized the preset goals.

An optimizer with low computational resource consumption is suitable for vacuum electronics optimization problems with well-defined performance targets. However, optimizing the device for the best performance is challenging. The optimal performance value cannot be set in the goals as evaluating the device performance before the design is difficult. In addition, repeatedly executing Optimizer by constantly adjusting the goals to approach the optimal performance value and obtain the optimal structural parameters is challenging, and the calculation is significantly cumbersome and time consuming. Conversely, the automatic optimization algorithms built into Optimizer are mechanical and rigid, and some algorithms cannot obtain the global optimal solution, such as Nelder Mead Simplex Algorithm and Interpolated Quasi Newton. Thus, Optimizer faces difficulties in solving complex and flexible multi-parameter and multi-objective vacuum electronic equipment optimization design problems.

3.3. NSGA-II

NSGA-II is an excellent multi-parameter multi-objective optimization algorithm. It is widely used to solve some large-dimensional, multimodal complex problems in science and engineering. MATLAB can be connected to CST PS using component object model (COM, a software architecture that allows one application to control component objects exported by another application) and ActiveX statements (an architecture that facilitates interoperability among software components implemented in different programming languages) in MATLAB (Haupt, 2008). The VBA language written in MATLAB can control CST PS for modeling and simulation and return the simulation results of CST PS for post-processing.

The structural parameters corresponding to those in CST PS were defined in MATLAB (Section 2.3) and used as decision variables of the NSGA-II. The anode electron number, electron focus size, and transit time (Section 2.4) calculated by CST PS were exported as the objective functions in NSGA-II. *pop* was 50, *gen* was 50, and computations required 193386 s. The iterative calculation results are as follows.

Fig. 8 shows the distribution of structural parameters of individuals in the population before and after 50 generations of inheritance. Fig. 8 (a) shows the distribution of structural parameters of each individual in

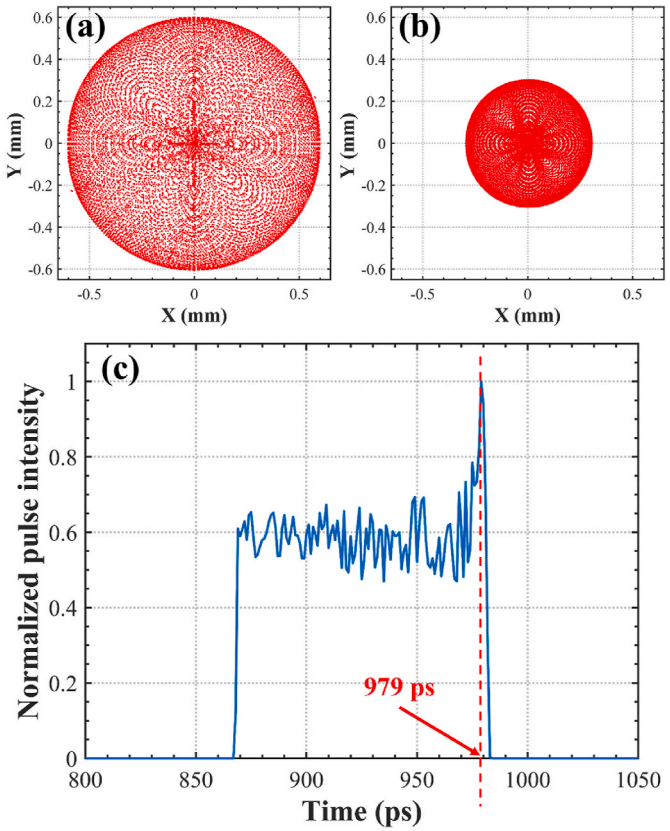

Fig. 7. Target results after optimization. (a) Electron focus under three optimized parameters. (b) Electron focus under six optimized parameters. (c) Electron transit time.

the initial population. When the population was initialized, the algorithm uniformly sampled the values of each structural parameter within the sampling interval to ensure the diversity of species in the population. After 50 generations of genetic evolution, the structural parameters in the population finally converged to a fixed value or several values, as shown in Fig. 8(b). For example, z_b and r_{in} converged to ~1 or 3 mm and ~15 mm, respectively. Thus, after 50 generations of iterative calculations, the optimal values of the two structural parameters in this population were determined.

The effect of *pop*, which required a computation time of 370374 s, on the optimization was further analyzed. The changes in the objective function frontier were comparatively analyzed for different population sizes and different numbers of iterations. The results are shown in Fig. 9 (a). When the iteration proceeded to 30 generations, the objective function value converged. By the 50th generation, the objective function exhibited a relatively uniform frontier. However, owing to insufficient population samples, this frontier is missing in the circled area. As shown in Fig. 9(b), when the population size increased, the frontier fitted by the red dashed line became smoother and contained more optimal solutions (Rosenthal and Markus, 2014; Zhang et al., 2021). According to the results, the increase in population size helped obtain a comprehensive set of optimal solutions in the entire problem space.

The optimal solution sets obtained by NSGA-II iterative calculations are all non-dominated solutions, also called the Pareto optimal solution. These optimal solutions have their advantages under different optimization objectives. They provide users with a solution library, from which users can select the solution that suits them according to actual applications or needs. Compared with a set of structural parameter results optimized by Optimizer according to a given goal, NSGA-II can provide users with a comprehensive and flexible set of parameter combinations to meet different performance and application requirements for vacuum electronic devices.

Weighing the three objective function values (Section 2.4), three sets of structural parameter schemes were selected from the optimal solution ($pop = 50$) for X-ray tube performance analysis. The R_e of the three schemes was 100 %. Option 1 was focused on obtaining the smallest R_{fs} of the X-ray tube. Option 3 was focused on obtaining the best *TT*. In Option 2, both R_{fs} and *TT* were considered. The structural parameter values of the three schemes are listed in Table 2.

The focal spot and time performance of the three X-ray tube schemes obtained using NSGA-II optimization are shown in Figs. 10 and 11, respectively.

As shown in Fig. 11, Option 3 exhibited the best time performance, with $TT = 0.71$ ns and $TTS = 85$ ps. This result can provide a structural design reference for some devices that require ultrafast response.

As can be inferred from Table 3, compared with Optimizer, the focal spot (radius = 0.17 mm) obtained by NSGA-II (NSGA-II Option 1) was 45 % smaller than the 0.31 mm obtained by Optimizer 2. Thus, the results obtained by Optimizer were not optimal. In addition, the solution set of the optimal structural parameters obtained based on NSGA-II can cope with various X-ray tube designs with special performance requirements. Option 1 is ideal if the X-ray tube has higher spatial resolution performance requirements. Option 3 is preferable if the X-ray tube has demands for temporal resolution performance. The flexibility of the NSGA-II optimization method can be extended to other vacuum electronic devices in addition to X-ray tubes. Although the NSGA-II algorithm demonstrates better optimization than Optimizer, it consumes more computational resources. The method used in our previous work (Yu et al., 2024) was applied to optimize the focusing structure of a

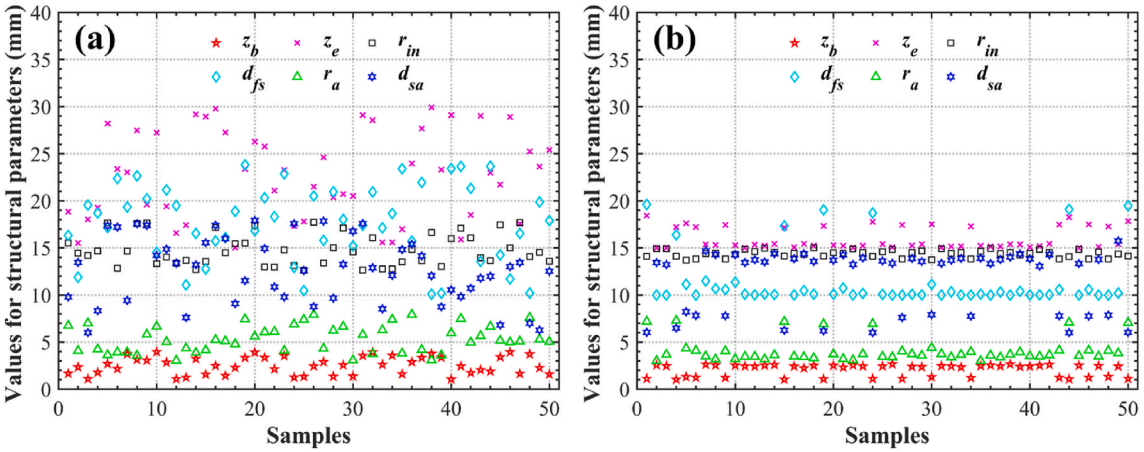

Fig. 8. Numerical distribution of structural parameters of individuals in the population. (a) Initial population. (b) Final population.

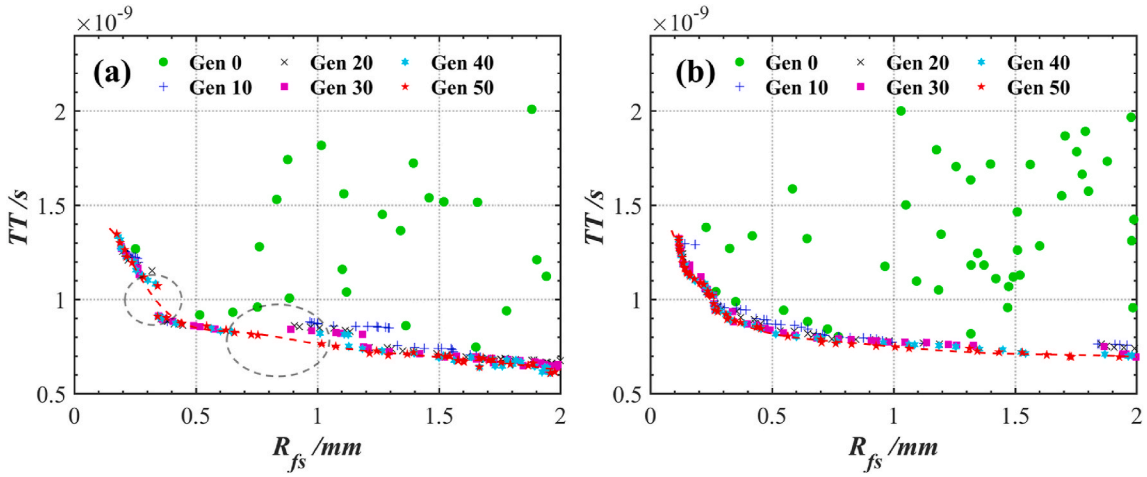

Fig. 9. Objective function frontier (*TT* vs. R_{fs}) at different iterations. (a) *pop* = 50. (b) *pop* = 100. The red dashed line is the 50th generation data fitting curve.

Table 2
Structural parameters corresponding to the three Options (*pop* = 50).

Options	z_b (mm)	z_e (mm)	r_{in} (mm)	d_{fs} (mm)	r_a (mm)	d_{sa} (mm)
Option 1	1.11	18.42	14.10	19.62	7.18	6.03
Option 2	1.22	17.48	13.83	10.58	4.11	7.78
Option 3	2.43	15.40	14.35	10.19	3.82	15.74

photocathode X-ray tube. The experimental results show that when the focusing electrode voltage is set to 2 kV, the prototype achieves an optimal focal spot of 0.53 mm × 0.79 mm, which is of the same order of magnitude as the simulated focal spot of 0.26 mm × 0.80 mm, thereby validating the effectiveness of the optimization algorithm.

4. Conclusion

In this work, an X-ray tube model was constructed based on CST PS, and its design was optimized using Par. Sweep, Optimizer, and NSGA-II algorithms. The optimization effects of the three methods were compared.

The results indicated that NSGA-II demonstrated the best optimization effect by achieving a focus radius of 0.17 mm and improving spatial resolution performance by 79.3 % and 45.2 %, compared with the other two methods. In addition, NSGA-II Option 3 provided a structural design with the best temporal performance, with a transition time and transition time spread of 0.71 ns and 85 ps, respectively. Nevertheless, NSGA-II consumed enormous computational resources. From the perspective of applicability, Par. Sweep is suitable for exploring the device performance changes with structural parameters or for simple optimization problems with a single target and two or fewer parameters. However, it is prone to falling into local optima during the optimization process. Optimizer can complete the specified optimization tasks and is suitable for vacuum electronic equipment optimization problems with clear performance indicators, aiming to achieve a given effect or a preset goal. Compared with the above two methods, NSGA-II is flexible in providing users with a solution package from which users can select the most suitable options according to their application needs. NSGA-II intelligent algorithm in combination with CST PS for optimization can provide a comprehensive optimization scheme and significantly enhances device design accuracy, effectively addressing issues related to low optimization precision and incomplete results in X-ray tube design. In the future, by improving the NSGA algorithm or simplifying the model structure in CST PS, it is expected that optimization time can be further reduced, thereby accelerating the rapid development of high-performance vacuum electronic devices.

CRediT authorship contribution statement

Hao Yu: Writing – original draft, Methodology, Software, Data curation, Visualization, Formal analysis. **Yunpeng Liu:** Resources, Supervision, Conceptualization, Writing – review & editing, Methodology. **Junxu Mu:** Writing – review & editing. **Jiaxin Bai:** Writing – review & editing. **Ao Xia:** Writing – review & editing. **Xiushan Wang:** Writing – review & editing. **Xiaobin Tang:** Project administration, Writing – review & editing, Supervision.

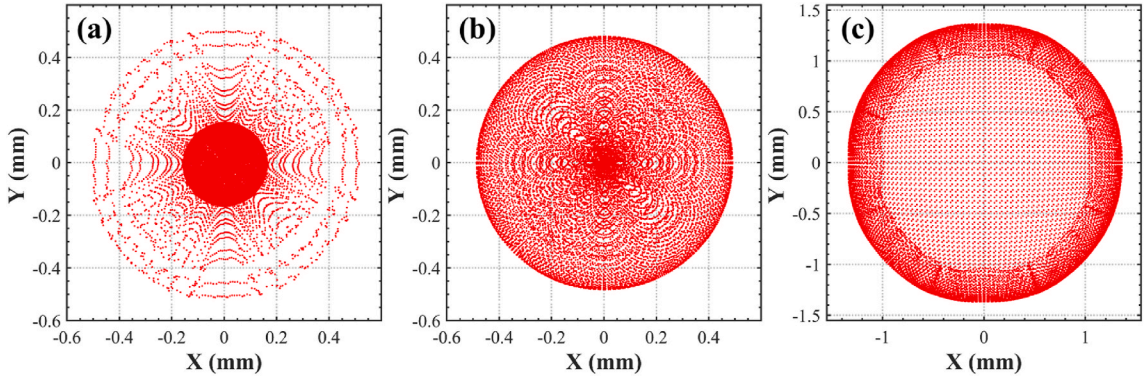

Fig. 10. Electron focal spot of X-ray tube under three Options. (a) Option 1. (b) Option 2. (c) Option 3.

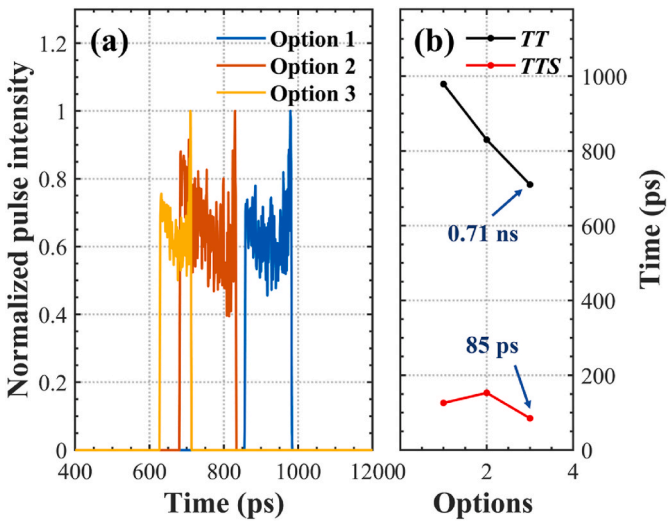

Fig. 11. Time performance of X-ray tube under three options. (a) Normalized pulse intensity of electrons arriving at the anode target at different times. (b) Transit time and transit time expansion.

Table 3
Optimizer vs. NSGA-II Optimization.

Parameters	Schemes	R_{fs} (mm)	*TT* (ns)	*Computational time* (s)
Pop = 50	Optimizer 1	0.60	–	33039
	Optimizer 2	0.31	0.98	1697
	NSGA-II Option 1	0.17	0.98	193386
	NSGA-II Option 2	0.44	0.83	
	NSGA-II Option 3	1.24	0.71	
Pop = 100	–	–	–	370374

Declaration of competing interest

The authors declare that they have no known competing financial interests or personal relationships that could have appeared to influence the work reported in this paper.

Acknowledgments

This work was supported by the National Natural Science Foundation of China (Grant No. 12375256), the Fundamental Research Funds for the Central Universities (Grant No. NT2023012) and the Postgraduate Research & Practice Innovation Program of NUAA (Grant No. xcxjh20230621). The authors would like to thank Xiaoyu Dong, Yingsheng Ni, Kun Zhang from IRay Electric Vacuum Technology (Nanjing) Co., Ltd., Nanjing, 210016, China for providing experimental results that supported the revision of this work.

Data availability

Data will be made available on request.

References

Antonsen, T.M., Mondelli, A.A., Levush, B., Verboncoeur, J.P., Birdsall, C.K., 1999. Advances in modeling and simulation of vacuum electronic devices. Proc. IEEE 87, 804–839. https://doi.org/10.1109/5.757256.

Cai, Y., Hao, R., Yu, S., Wang, C., Hu, G., 2020. Comparison of two multi-objective optimization methods for composite radiation shielding materials. Appl. Radiat. Isot. https://doi.org/10.1016/j.apradiso.2020.109061.

Deb, K., Pratap, A., Agarwal, S., Meyarivan, T., 2002. A fast and elitist multiobjective genetic algorithm: NSGA-II. IEEE Trans. Evol. Comput. 6, 182–197. https://doi.org/10.1109/4235.996017.

Feng, Z., Liu, Y., Mu, J., Chen, W., Lai, S., Tang, X., 2022. Optimization and testing of groove-shaped grid-controlled modulated X-ray tube for X-ray communication. Nucl. Instrum. Methods Phys. Res. Sect. A Accel. Spectrom. Detect. Assoc. Equip. 1026, 166218. https://doi.org/10.1016/j.nima.2021.166218.

Figueroa, R., Geser, F., López-Correa, J., Malano, F., Valente, M., 2021. Monte carlo study of a convergent X-ray beam for high resolution X-ray fluorescence imaging. Appl. Radiat. Isot. https://doi.org/10.1016/j.apradiso.2021.109610.

Fox, J., Hyoung, K.L., 2024. Simulation study of electron beam optics for a distributed X-ray source toward stationary CT architecture. Nucl. Instrum. Methods Phys. Res. Sect. A Accel. Spectrom. Detect. Assoc. Equip. 1062, 169149. https://doi.org/10.1016/j.nima.2024.169149.

Gao, Y., Wu, Y., Li, S., Hei, D., Tang, Y., 2024. Design of a multi-carrier X-ray Source for Communication with Energy Modulation Information, 1–13. XST. https://doi.org/10.3233/XST-240094.

Gui, J., Chen, Y., Hong, X., Wu, PeterZ., Hu, Z., Liang, D., Zheng, H., 2015. Design of electrostatic focusing lens for an X-ray source with carbon nanotube cathode. J. Med. Imaging Health Inform. 5, 1462–1466. https://doi.org/10.1166/jmihi.2015.1568.

Hang, S., Liu, Y., Li, H., Tang, X., Chen, D., 2018. Temporal characteristic analysis of laser-modulated pulsed X-ray source for space X-ray communication. Nucl. Instrum. Methods Phys. Res. Sect. A Accel. Spectrom. Detect. Assoc. Equip. 887, 18–26. https://doi.org/10.1016/j.nima.2018.01.031.

Haupt, R.L., 2008. Using MATLAB to control commercial computational electromagnetics software. Appl. Comput. Electromagn. Soc. J. 23, 98. https://doi.org/10.1080/08839510701821652.

Ihsan, A., Heo, S.H., Cho, S.O., 2007. Optimization of X-ray target parameters for a high-brightness microfocus X-ray tube. Nucl. Instrum. Methods Phys. Res. Sect. B Beam Interact. Mater. Atoms 264, 371–377. https://doi.org/10.1016/j.nimb.2007.09.023.

Jiye, X., 1987. Theoretical research on electron optics. J. Electron. Microsc. Tech. 7, 331–336. https://doi.org/10.1002/jemt.1060070413.

Li, Y., Zhao, Q., Li, Z., Yuan, X., Zong, Y., Li, J., Cao, S., Long, Y., Zhang, Z., 2023. Beam dynamics optimization design of rhodotron electron accelerator based on genetic algorithm and sensitivity analysis. Appl. Radiat. Isot. 201, 111024. https://doi.org/10.1016/j.apradiso.2023.111024.

Mistry, K.K., Lazaridis, P.I., Zaharis, Z.D., Akinsolu, M.O., Liu, B., Xenos, T.D., Glover, I. A., Prasad, R., 2019. Time and frequency domain simulation, measurement and optimization of log-periodic antennas. Wirel. Pers. Commun. 107, 771–783. https://doi.org/10.1007/s11277-019-06299-w.

Parmee, R.J., Collins, C.M., Milne, W.I., Cole, M.T., 2015. X-ray generation using carbon nanotubes. Nano. Converg. 2, 1. https://doi.org/10.1186/s40580-014-0034-2.

Rosenthal, S., Markus, B., 2014. Impact of population size and selection within a customized NSGA-II for biochemical optimization assessed on the basis of the average cuboid volume indicator. Proceedings of Sixth International Conference on Bioinformatics, Biocomputational Systems and Biotechnologies. BIOTECHNO. https://doi.org/10.1055/s-2007-970006, 2014.

Srinivas, N., Deb, K., 1994. Muiltiobjective optimization using nondominated sorting in genetic algorithms. Evol. Comput. 2, 221–248. https://doi.org/10.1162/evco.1994.2.3.221.

Tan, C., Tang, C., Huang, W., Jin, Q., Du, Y., Luo, Q., Wu, P., Liu, D., Zhang, L., Xu, C., 2019. Beam simulation and experiment of multi-focal spot electron gun for distributed X-ray sources. Nucl. Instrum. Methods Phys. Res. Sect. A Accel. Spectrom. Detect. Assoc. Equip. 920, 43–49. https://doi.org/10.1016/j.nima.2018.11.039.

Yu, H., Liu, Y., Wang, X., Mu, J., Bai, J., Xia, A., Wang, K., Tang, X., 2024. Design and testing of metal photocathode X-Ray source based on microchannel plate. IEEE Trans. Electron. Dev. 71, 7099–7105. https://doi.org/10.1109/TED.2024.3465463.

Zhang, P., Qian, Y., Qian, Q., 2021. Multi-objective optimization for materials design with improved NSGA-II. Mater. Today Commun. 28, 102709. https://doi.org/10.1016/j.mtcomm.2021.102709.